Geophysical Research Letters

RESEARCH LETTER
10.1029/2024GL112179

Special Collection:
Space Weather Events of 2024 May 9-15

Mesosphere and Lower Thermosphere Temperature Responses to the May 2024 Mother's Day Storm

Xiao Liu[1,2], Jiyao Xu[2,3], Jia Yue[4,5], Wenbin Wang[6], and Juliano Moro[7]

[1]School of Mathematics and Statistics, Henan Normal University, Xinxiang, China, [2]State Key Laboratory of Space Weather, National Space Science Center, Chinese Academy of Sciences, Beijing, China, [3]University of the Chinese Academy of Science, Beijing, China, [4]NASA Goddard Space Flight Center, Greenbelt, MD, USA, [5]Physics Department, Catholic University of America, Washington, DC, USA, [6]High Altitude Observatory, National Center for Atmospheric Research, Boulder, CO, USA, [7]Southern Space Coordination—COESU/INPE/MCTI, Santa Maria, Brazil

Abstract The storm-time temperature difference with respect to its quiet-time expectation (ΔT) in the mesosphere and lower thermosphere were studied during the extreme storms on 2024 Mother's Day and 2003 Halloween Day. The storm-time ΔT were determined by performing daily zonal running mean on the temperature profiles in the ascending and descending nodes separately. The storm-time ΔT had peak values of ≥25 K and extended downward to ∼100 km globally. Above 105 km, the global mean ΔT had values of ≥20 K in the early morning and of ≥15 K in the late afternoon during storm-time. At high latitudes, the storm-time ΔT was larger in the late afternoon than in the early morning. This is opposite to that at middle and low latitudes. Adiabatic warming/cooling caused by the heating-induced circulation changes outside of the auroral oval is likely responsible for the local time and latitude dependence of the storm-time ΔT.

Plain Language Summary The storm-time energy input in the auroral oval plays an important role in changing the dynamics and electrodynamics of the neutral atmosphere and ionosphere. Although the energy input due to Joule and particle heating is the strongest at high latitudes, its influences are global. The mesosphere and lower thermosphere are transition regions between the middle atmosphere and the ionosphere, which are affected by the lower atmosphere, the ionosphere, and the solar and geomagnetic activities. This complicates the physics and dynamical structures of the mesosphere and lower thermosphere during the storm-time, especially the two extreme storms in the past 20 years. The temperature measured by SABER is used to study the local time and latitude dependence of the storm-time temperature difference with respect to its quiet-time expectation. The extreme storms are rare with average occurrence frequency of about 4 days per 11-year. The storm-time temperature difference was larger in the late afternoon than in the early morning at high latitudes, which is opposite to that at middle and low latitudes. This highlight that the extreme storms induce much larger and observable temperature changes as compared with those associated tides.

Key Points:

- The temperature increased globally and depended on local time during extreme storms on the 2024 Mother's Day and 2003 Halloween Day
- The storm-time temperature difference (ΔT) had global means of ≥20 K in the early morning and of ≥15 K in the late afternoon
- The ΔT is larger in the late afternoon than in the early morning at high latitudes, but the reverse is true at middle and low latitudes

Correspondence to:
J. Xu,
xujy@nssc.ac.cn

Citation:
Liu, X., Xu, J., Yue, J., Wang, W., & Moro, J. (2025). Mesosphere and lower thermosphere temperature responses to the May 2024 Mother's Day storm. *Geophysical Research Letters*, *52*, e2024GL112179. https://doi.org/10.1029/2024GL112179

Received 11 SEP 2024
Accepted 10 JAN 2025

Author Contributions:
Conceptualization: Xiao Liu, Jiyao Xu, Jia Yue, Wenbin Wang
Data curation: Xiao Liu, Jia Yue
Formal analysis: Xiao Liu
Investigation: Xiao Liu
Methodology: Xiao Liu, Jiyao Xu, Jia Yue, Wenbin Wang
Validation: Xiao Liu
Writing – original draft: Xiao Liu
Writing – review & editing: Jiyao Xu, Jia Yue, Wenbin Wang, Juliano Moro

1. Introduction

Geomagnetic storms have strong impacts on the ionosphere, thermosphere, and even on the mesosphere with a significant amount energy and momentum input from the magnetosphere. This increases polar cap thermosphere temperature and changes neutral winds and densities at high latitudes through Joule heating and heating by energetic precipitating particles, and ion drag (Banks, 1979; Killeen, 1987; Rees et al., 1983; Roble et al., 1987). The dynamic changes at high latitudes are then transmitted equatorward changing the dynamic and thermal structures of the thermosphere at middle and low latitudes through ion-neutral coupling and global circulation changes (Burns et al., 1992, 1995; Lei et al., 2011; H. Liu & Lühr, 2005; Rees et al., 1983; Richmond, 1979; W. Wang et al., 2008; Zesta & Oliveira, 2019). On the other hand, geomagnetic storms enhance thermosphere infrared emission, which plays a cooling effect on the thermosphere (Mlynczak et al., 2018, 2024). This complicates the physics and dynamical structures of the mesosphere and lower thermosphere (MLT) during the storm-time. Ground-based and satellite observations showed that the storm-time temperature in the MLT region could be warmer or cooler or display no change as compared to the quiet-time (N. Wang et al., 2021 and references there in). The MLT is the transition region between the middle atmosphere and the thermosphere and ionosphere. It is influenced by the dynamics from the lower atmosphere and from the thermosphere and ionosphere, the energy input caused by solar and geomagnetic activities (H.-L. Liu, 2016), as well as the competition between energy input and radiative cooling. This suggests the importance and complexity of storm-time temperature difference

with respect to its quiet-time expectation (ΔT) in the MLT (X. Liu et al., 2018; Pancheva et al., 2007; Sun et al., 2024; Tyssøy et al., 2010; von Savigny et al., 2007; N. Wang et al., 2021).

The simulation results using the Thermosphere Ionosphere Mesosphere Electrodynamics General Circulation Model (TIME-GCM) showed that the storm-time ΔT at middle latitudes is caused by the adiabatic heating/cooling due to the changes in circulation and vertical winds in the MLT (Li et al., 2018). Further studies showed that the horizontal wind changes in the middle-latitudes upper thermosphere cause a downward vertical wind, that induces adiabatic heating in the MLT. Then, the increasing temperature induces upward wind, which decreases temperature through adiabatic cooling and induces a poleward wind at higher latitudes (Li et al., 2019). It should be noted that Joule heating is a major heat source above the auroral oval, where electric fields are the strong (Li et al., 2023; Roble et al., 1987; W. Wang et al., 2012; Xu et al., 2013). At high latitudes, the storm-time ΔT is weaker at 00:00–12:00 LT (local time, dawn sector) than at 12:00–24:00 LT (dusk sector) during the initial and main phases. This indicates that the storm-time ΔT depends on latitudes and local times (LTs) (Li et al., 2023). Using the temperature measured by SABER (Sounding of the Atmosphere using Broadband Emission Radiometry) during 2002–2023, Yamazaki et al. (2024) showed that the high latitude storm-time ΔT is larger in the dusk sector than in the dawn sector. The dusk-dawn asymmetry of the storm-time ΔT has also been revealed by Wei et al. (2024) based on the SABER temperature data in 54 geomagnetic storms in 2002–2021. These studies on the LT dependent, storm-time ΔT is mainly focused on high latitudes, where the Joule heating effects are comparable to the adiabatic heating and vertical heat advection above 100 km (Li et al., 2023).

The increased temperature in the auroral oval induces an upward and divergent flow in the auroral oval region. This divergent flow induces meridional circulations (short for the storm-induced circulation) in the directions of both poleward and equatorward relative to the auroral oval (Li et al., 2019, 2023; W. Wang et al., 2008). The storm-induced circulation competes with the meridional circulation caused by solar heating induced pressure gradient force. This competition results in LT-dependent, storm-time ΔT. In this work, the storm-time ΔT in the MLT during strong storms will be investigated to reveal their LT and latitude dependences. One G5 superstorm commenced on 10 May 2024 (around Mother's Day). The three-hourly ap index reached its peak of 400 nT at 01:30 UT (universal time) and 07:30 UT on May 11. For comparison, the storm-time ΔT in the MLT will also be discussed during the Halloween storm occurred during late October 2003. The three-hourly ap index reached its peak of 400 nT at 07:30 UT on October 29 and at 19:30 UT on October 30. During the two superstorms, the temperature measured by the SABER instrument covered a latitude range of 50°S–82°N. These observations provide a good opportunity to study the LT and latitude dependences of the storm-time ΔT in the MLT.

2. Data and Methods

The temperature profiles measured by SABER are in the latitude range of 83°N–52°S or 52°N–83°S depending on satellite yaw cycles (Esplin et al., 2023; Russell et al., 1999). For the Level 2A data, the precision of a single temperature profile is of ∼3.3–10.5 K at 90–110 km with a vertical resolution of 2 km as summarized at https://spdf.gsfc.nasa.gov/pub/data/timed/saber/ (Dawkins et al., 2018; Remsberg et al., 2008). The SABER temperature product is stable after resolving the issue of algorithm instability (Mlynczak et al., 2020, 2022, 2023) and is suitable to study the responses of the MLT temperature to superstorms.

The method of determining storm-time temperature difference with respect to its quiet-time expectation (ΔT) is summarized in Figure 1. The three-hourly ap index (top of Figure 1a) increased from 179 nT at 16:30 UT on May 10th to 400 nT at 01:30 UT and 07:30 UT on May 11th, and decreased to 12 nT at 16:30 UT on May 13th. The hourly Dst index (middle of Figure 1a) decreased from −32 nT at 19 UT on May 10th to −412 nT at 03 UT on May 11th. The hourly AE index (provisional version) reached peaks of 1807 nT at 19 UT on May 10th and 1956 nT at 09 UT on May 11th (not shown, https://wdc.kugi.kyoto-u.ac.jp). The detailed interplanetary and geomagnetic environment can be found in Lazzús and Salfate (2024). The temperature profiles at 50°N are taken as an example to show the procedure of isolating the temperature variations caused by storm and other factors. Here the latitude band has width of 10° without any overlap. The centers of the latitude bands are from 80°S to 50°N. The bottom row of Figure 1a shows the LTs of SABER samplings in the ascending (black) and descending (red) nodes at 50°N, respectively. The LT differences are approximately 13–15 (or 9–11) hours between the ascending and descending nodes. Such that the LT dependence of the storm-time ΔT can be studied by analyzing the temperature in the ascending and descending nodes, respectively.

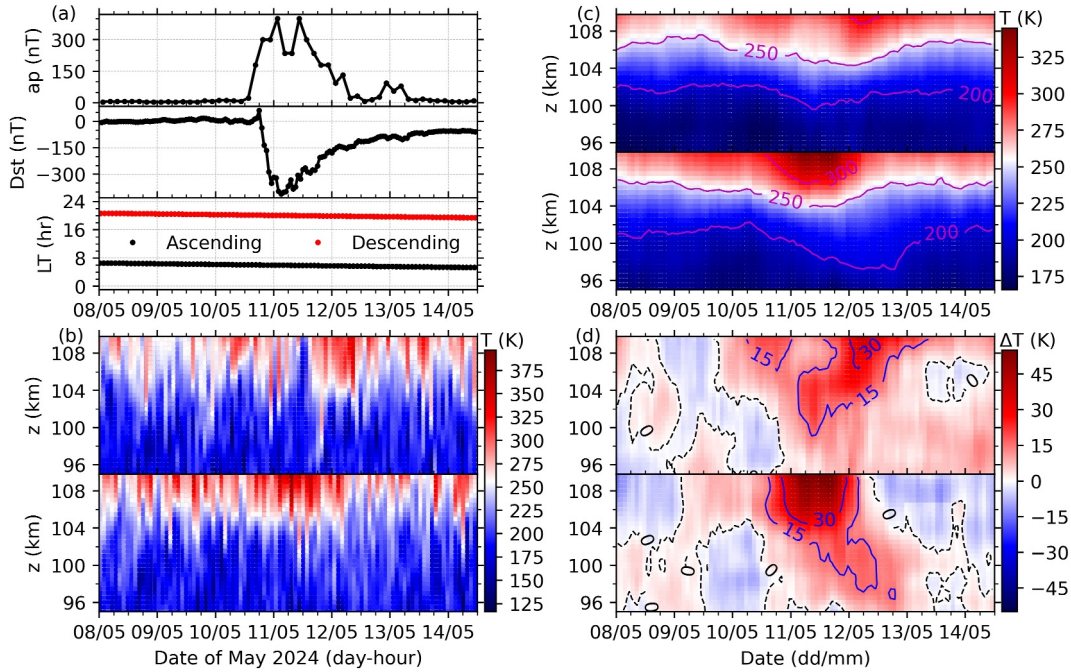

Figure 1. Geomagnetic indices and SABER mesosphere and lower thermosphere temperatures from May 8th to 14th, 2024. (a): Three-hourly ap index (top), hourly Dst index (middle), local time (LT) of SABER samplings (bottom); (b): SABER temperature at 50°N in the ascending (top) and descending (bottom) nodes; (c): same as panel (b) but for the daily zonal running mean temperature; (d): same as panel (b) but for the temperature difference with respect to its quiet-time expectation (see text for detail).

The raw temperature profiles shown Figure 1b are generally warmer during the storm-times (i.e., from 12 UT on 10th to 12 UT on 12th May) as compared to that during the quiet-times (i.e., from 00 UT on 8th to 12 UT on 10th May). However, there are also warmer temperature profiles during quiet-times. Thus, it is necessary to isolate the temperature variations caused by storm from those caused by tides, gravity waves or other processes. Being different from the method of Liu et al. (2018) and Wang et al. (2021), who perform daily zonal running mean on the raw temperature profiles in the ascending and descending nodes together. Here, the daily zonal running mean (Figure 1c) is performed separately in the ascending and descending nodes to remove the non-migrating tides and gravity waves (X. Liu et al., 2014, 2017; Xu et al., 2014). However, the migrating tides cannot be removed efficiently due to the limited LT coverage around the storm-times. SABER observations revealed that the peaks of the migrating tides have magnitudes of ∼10–20 K around the Equator and ∼4–12 K at middle latitudes in February–March and August-September and below 100 km. Moreover, the amplitudes of migrating tides decrease to less than ∼10 K above 100 km (Mukhtarov et al., 2009; Xu et al., 2009; Zhang et al., 2006). Ground-based lidar observations revealed that the amplitudes of tides are generally less than 10 K at middle latitudes and ∼2–4 K at high latitudes (Lübken et al., 2011; Yuan et al., 2006, 2008). These magnitudes are much smaller than the temperature enhancement (≥15 K) caused by the storm and do not affect our analysis below. The storm-time temperature difference with respect to its quiet-time expectation (ΔT, Figure 1d) are calculated by subtracting the quiet-time temperature baseline (i.e., the average temperature from 00 UT on 8th to 12 UT on 10th in May) from the daily zonal running mean temperature profiles at each latitude band. Figure 1d shows that the storm-time ΔT has magnitudes of ≥30 K above 105 km and of ≥15 K above 98 km at 50°N.

3. Morphology of Storm-Time Temperature Differences

To examine the storm-time ΔT in the MLT more comprehensively, the storm-time ΔT during the 2003 Halloween storm is calculated in a same manner as that described in Section 2. During the 2003 Halloween storm, the 3-hourly ap index (top of Figure 2a) reached its maximum of 400 nT on October 29th and 30th, 2003. The Dst index (middle of Figure 2a) reached its minima of −350 nT on October 29th and −383 nT on October 30th. Previous studies have showed that the 2003 Halloween storm have important effects on space weather (Lei

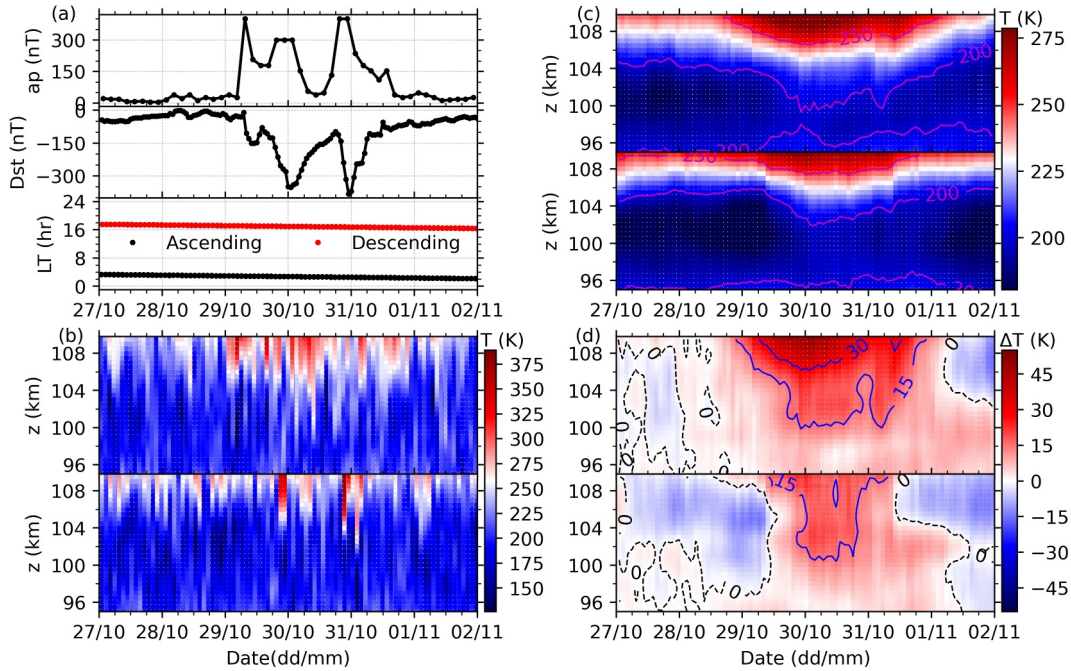

Figure 2. Same caption as Figure 1, but for the 2003 Halloween storm. (a) Three-hourly ap index (top), hourly Dst index (middle), local time (LT) of SABER samplings (bottom). The upper and lower panels in panels (b–d) show the results in the ascending and descending nodes, respectively. The quiet-time baseline is defined as the average temperature from 00 UT on 27th to 12 UT on 28th in October 2003.

et al., 2011; Pulkkinen et al., 2005). Here we focus on the storm-time ΔT in the MLT. Figure 2b shows that the raw temperatures are generally warmer during the storm-times as compared to that during quiet-times. The warmer temperatures during the storm-times are more obvious after removing the variations caused by tides, gravity waves or other factors (Figure 2c). The storm-time ΔT at 50°N (Figure 2d) has magnitudes of ≥30 K above 106 km in the early morning (ascending node) and of ≥15 K above 102 km in the early morning (ascending node) and in the late afternoon (descending node). Comparisons between Figures 1d and 2d show that the storm-time ΔT at 50°N are larger and lasted shorter during the 2024 Mother's Day storm than that during the 2003 Halloween storm. One possible reason is that the 2024 Mother's Day storm was stronger (with daily Ap index of 273 nT and Dst of −292 nT) and lasted only for one day (May 11th). Compared to the 2024 Mother's Day storm, the 2003 Halloween storm was relatively weaker and longer lasting (from 29th to 31st October). The Ap values during the 2003 Halloween storm for the 3 days were of 204, 191, and 116 nT, respectively (Mlynczak et al., 2024). Another possible reason is that the SABER observations are at different LTs and in different months. The LTs of SABER observations are around 05:27 and 20:32 during the 2024 Mother's Day storm and are around 02:09 and 17:22 during the 2003 Halloween storm. The circulations may be different during the two storms.

Figure 3 shows the global maps of storm-time ΔT and quiet-time ΔT during the 2024 Mother's Day storm at 109 and 98 km in the ascending (left two columns) and descending (right two columns) nodes during. Figure 3 shows that the quiet-time ΔT has global means of ∼0 K at the two heights. In contrast, the global means of the storm-time ΔT are positive, but decrease from ∼27 K at 109 km to ∼3 K at 98 km. This indicates that the 2024 Mother's Day storm increases the temperature globally in the MLT. The maxima of the storm-time ΔT are several times larger than the quiet-time ΔT at the two heights. Further examination can be found that the variations of the storm-time ΔT are almost uniform in each zonal circle. This indicates that the storm-time ΔT is enhanced globally (all the zonal circles from 80°N to 50°S). The enhancements are more prominent at 109 km than those at 98 km in both nodes. The global enhancements and the uniform in all zonal circles of the storm-time ΔT can also be found during the 2003 Halloween storm (not shown here).

Focusing on the storm-time ΔT, we see that the magnitudes of ΔT depend on latitudes and LTs (referring to the ascending and descending nodes). At latitudes poleward of 50°N, the maxima of ΔT at the two heights are around

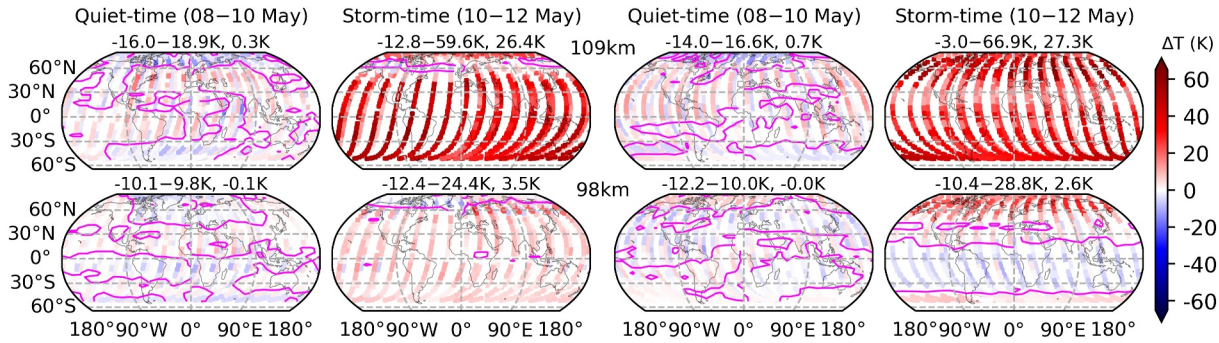

Figure 3. Global maps of storm-time ΔT (the second and fourth columns) and quiet-time ΔT (the first and third columns) around the 2024 Mother's Day at four heights (109 and 98 km) in the ascending (left two columns) and descending (right two columns) nodes. The mean local time (hh:mm) and its standard deviation (mm, unit of minute) around the Equator are labeled on the top of each panel with the form of "hh:mm ± mm." The minimum, maximum and the mean of global ΔT are labeled on the top of each panel. The magenta contour lines indicate the ΔT = 0.

10–20 K in the ascending node (05:27 LT, early morning). While in the descending node (20:32 LT, later afternoon), the maxima of ΔT at the two heights decrease from ∼67 K at 109 km to ∼29 K at 98 km. At 40°S–40°N and at the two heights, the magnitudes of ΔT are generally larger in the ascending node than those in the descending node. This indicates that the LT-dependence of the storm-time ΔT is a function of latitudes. Specifically, the storm-time ΔT is larger in the descending node than in the ascending node at latitudes poleward of 50°N, but is larger in the ascending node than in the descending at 40°S–40°N. The storm-time ΔT exhibits hemispheric asymmetry. In the ascending node, the mean ΔT is ∼37 K at 0°–40°S and 109 km, which is larger than the ∼28 K at 0–40°N at the same height. However, the mean ΔT is larger at 0–40°N than at 0°–40°S below 105 km. In the descending node, the mean ΔT is larger at 0°–40°S than at 0–40°N above 105 km and is larger at 0–40°N than at 0°–40°S below 100 km. The hemispheric asymmetry at higher heights is consistent with the superimposed epoch analysis by N. Wang et al. (2021) based on 59 coronal mass ejection (CME) events during 2003–2013. They showed that the storm-time ΔT is larger in the southern hemisphere than that in the northern hemisphere for the CME induced storms.

4. Discussions

Both the 2024 Mother's Day storm and the 2003 Halloween storm were caused by CMEs and were classified as extreme storms. The extreme storms are categorized as G5 and have average occurrence frequency of about 4 days per 11-year solar cycle as reported by NOAA space weather prediction center. The temperature measured by SABER covered two solar cycles (2002–2024). During the two solar cycles, there were only two extreme storms (Gonzalez-Esparza et al., 2024). These extreme storms are rare and the induced ΔT are more observable and larger than tides. The LT dependence of storm-time ΔT can be observed distinctly. It should be noted that the LT dependence of storm-time ΔT may exist for all geomagnetic storms. However, it is difficult to quantify the temperature changes caused by minor storms because tidal signals are mixed with the storm responses during minor storms.

During these extreme storms, the strong energy input from the magnetosphere into the ionosphere and thermosphere changes the thermal structure in the MLT. Thus, the resultant storm-time ΔT during the two extreme storms are compared here to shed some light of physics. Figure 4 shows a polar view of the altitude-averaged storm-time ΔT in the height range of 100–109 km on the geomagnetic coordinates during the 2003 Halloween storm. Here the geomagnetic coordinates are transformed through the Altitude-Adjusted Corrected Geomagnetic (AACGM) coordinates (Shepherd, 2014). The similarities of the storm-time ΔT during the two extreme storms (Figures 3 and 4) are ascribed into the following two aspects. Firstly, the locations of the largest storm-time ΔT are not at the highest latitude but around 60°N generally. Moreover, the storm-time ΔT around 60°N is larger in the descending node (later afternoon) than in the ascending node (early morning). This local time dependence of the storm-time temperature changes depends on how the upper atmosphere responds to the storm-time high latitude forcing that varies with location, geomagnetic local time and storm characteristics such as the storm strength, onset time and phase. This consistent with the climatology patterns that the storm-time temperature enhancements are larger in the dusk sector at high latitudes (Li et al., 2023; Wei et al., 2024; Yamazaki et al., 2024). In the southern hemisphere, the

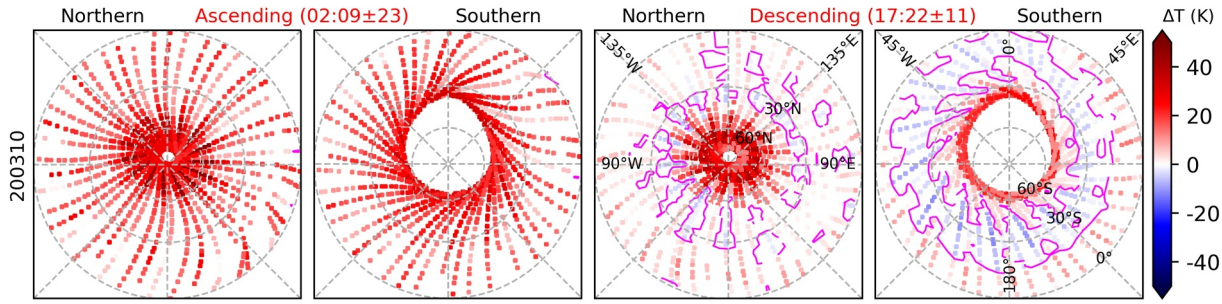

Figure 4. Polar view of the altitude-averaged storm-time ΔT in the height range of 100–109 km on geomagnetic coordinates during the 2003 Halloween storm. The left and right two columns are the results in the ascending and descending nodes, respectively. The magenta contour lines indicate the ΔT = 0.

storm-time ΔT decreases from high latitudes to low latitudes. Secondly, at lower and middle latitudes, the storm-time ΔT in ascending node is larger than in the descending node.

The main difference of the storm-time ΔT between the two extreme storms can be ascribed as the following two aspects. (a) The storm-time ΔT are larger and lasting for a shorter period of time during the 2024 Mother's Day storm than that during the 2003 Halloween storm (Figures 1d and 2d). (b) The storm-time ΔT decreases with the decreasing latitudes more slowly during the 2024 Mother's Day storm than that during the 2003 Halloween storm, especially in the ascending node (Figures 3 and 4). The possible reasons for these differences may be the combination effects of following aspects. Firstly, the 2024 Mother's Day storm was strong and lasted only for one day. In contrast, the 2003 Halloween storm was relatively weaker and lasted for 3 days. Secondarily, the meridional circulation depends on LT and season, where the dynamical influences from the lower atmosphere cannot be neglectable in the MLT (H.-L. Liu, 2016). Moreover, heating and meridional circulation caused by different storms also vary with LT. Even in the same storm these changes also have LT dependence. This might enhance or suppress the storm-induced circulation, which is originated from the auroral oval and expand to other latitudes. Thirdly, the hemispheric asymmetry of the storm-time ΔT is only partially consistent with the superimposed epoch analysis by Wang et al. (2021) based on 59 CME events during 2003–2013. They also noted that a single storm can be different from the averaged results of multiple events.

The new observational result is that the storm-time ΔT is larger in the dawn sector (mainly from the mid-night to the early morning) than that in the dusk section (mainly in the later afternoon) at 40°S–40°N during the two extreme storms. This is in contrast to those at high latitudes, where the storm-time ΔT is larger in the dusk sector than in the dawn sector. It looks like that the latitude band of 50°N–60°N acts as a boundary, which separates the storm-time temperature enhancements having different LT and latitude dependencies. Specifically, the storm-time ΔT is larger in the dusk sector at high latitudes and in the dawn sector at middle and lower latitudes. The possible physics behind the new observational fact can be explained as below.

The thermal balance in the MLT region is achieved among Joule heating, heat transfer due to molecular and eddy diffusion, adiabatic heating/cooling caused by horizontal and vertical advections, and radiative cooling (Burns et al., 1992, 1995; Killeen, 1987). During the storm-time, Joule heating is the main driver of temperature enhancement in the auroral oval above about 100 km (Li et al., 2023; Roble et al., 1987; W. Wang et al., 2012; Xu et al., 2013). This is also supported by Figure 4, which shows that the temperature enhancements are mainly around 60°N but not within the entire polar cap or at lower latitudes above 100 km. The latitudes around 60°N coincide well with the auroral oval (Figure 2 of Landry & Anderson, 2019), where electric fields and auroral precipitation are strong too. This produces strong Joule heating. Because the auroral oval locates mainly in the latitude bands of 60°–70° but not in the entire polar cap, the temperature enhancements are mainly over the auroral oval but not in the entire polar cap. The enhanced temperature induces an upward (above the auroral oval) and divergent (away from the auroral oval) flow due to the thermal expansion. Then the upward and divergent flow causes perturbations to meridional winds both poleward and equatorward from the auroral oval. Here we refer to perturbations to meridional winds as the storm-induced circulation. On the other hand, the solar heating depends highly on LT, which contributes to establish the meridional circulation in the MLT. This meridional circulation can be regarded as the background, quiet-time circulation. The latitude and LT dependencies of storm-

time temperature changes are mainly caused by the competition effects between the storm-induced circulation and the quiet-time circulation.

During the daytime, the pressure gradient force is anti-sunward (i.e., northward in the northern hemisphere and southward in the southern hemisphere) due to the solar heating (Burns et al., 1995). We refer to the circulation established by the momentum balance between this force and other forcing processes as the quiet-time circulation. In the poleward direction of the auroral oval, the storm-induce circulation is reenforced by the quiet-time circulation during the daytime. This induces a faster poleward and downward circulation at higher latitudes. Then the downward motion increases temperature at higher latitudes. Equatorward direction of the auroral oval, the storm-induce circulation is suppressed by the quiet-time circulation in the daytime. This induces the weak temperature enhancements at middle and low latitudes. During the nighttime, the quiet-time circulation is sunward. The superposition of the equatorward, storm-induced circulation and the quiet-time circulation induces larger temperature enhancements at middle and low latitudes. However, the quiet-time circulation in the MLT region may not be the idea case as described above due to the significant dynamical influences (i.e., wave breaking and momentum deposition, day-to-day tidal variability) around the MLT and from the lower atmosphere. This might induce a complex dynamical structure in the MLT region (H.-L. Liu, 2016). The detailed physics behind the storm-time temperature changes are complex in the MLT region and should be explored through first principle numerical simulations (e.g., TIME-GCM or WACCM-X) in future research.

5. Conclusions

The 2024 Mother's Day storm is classified as an extreme storm and had a similar strength as that of the 2003 Halloween storm. These extreme storms are rare and the induced ΔT are more observable and larger than tides. Thus, the LT dependence of storm-time ΔT can be observed distinctly. Due to the rarity of the extreme storms, we cannot conclude this phenomenon is a commonly occurring feature, but it is a novel discovery. The temperature data from the SABER instrument are used to study the LT and latitude dependencies of the storm-time temperature changes in the MLT region. The storm-time temperature changes are determined by subtracting the daily zonal running mean of the temperature profiles in the ascending and descending nodes, respectively.

We found that the storm-time temperature enhancements occurred globally and are dependent on latitudes and LTs. The main results of this study are as follows: (a) The storm-time ΔT has peak values of $\geq$25 K and extended downward to $\sim$100 km globally. (b) Above 105 km, the storm-time ΔT has global means of $\geq$20 K in the early morning and of $\geq$15 K in the late afternoon. (c) The temperature enhancements are hemispherically asymmetric, which depends on heights and LT. (d) At high latitudes, the storm-time ΔT is larger in the later afternoon than in the early morning. At middle and low latitudes, the storm-time ΔT is larger in the early morning than in the later afternoon. (e) The adiabatic warming/cooling caused by the storm-induced circulation perturbations outside of the auroral oval and its competition with the quiet-time circulation may be the main physical process behind the local time and latitude dependency of the storm-time ΔT. However, other factors should not be excluded, such as the vertical and horizontal heat advections, heat conduction, heating by solar radiation and auroral precipitation, and radiative cooling, which all vary with local time and latitude during storms. Moreover, the dynamical structure in the MLT is complex even in the quiet-time, further simulation studies should be performed to further explore the exact physics behind the storm-time temperature changes regionally and globally.

Data Availability Statement

All SABER data can be accessed from Space Physics Data Facility, Goddard Space Flight Center (https://spdf.gsfc.nasa.gov/pub/data/timed/saber/, Mlynczak et al. (2023)). The tri-hourly ap index is downloaded from https://kp.gfz-potsdam.de/ (Matzka et al., 2021). The hourly Dst index is downloaded from https://wdc.kugi.kyoto-u.ac.jp/ (Saroso et al., 1993).

Acknowledgments
This work was supported by the Project of Stable Support for Youth Team in Basic Research Field of Chinese Academy of Sciences (Grant YSBR-018), the National Natural Science Foundation of China (42174196), the Informatization Plan of Chinese Academy of Sciences (CAS-WX2021PY-0101), and the Open Research Project of Large Research Infrastructures of CAS "Study on the interaction between low/mid-latitude atmosphere and ionosphere based on the Chinese Meridian Project." This work was also supported in part by the Specialized Research Fund and the Open Research Program of the State Key Laboratory of Space Weather. The National Center for Atmospheric Research is sponsored by the National Science Foundation. The storm scales and its rate can be found at https://www.swpc.noaa.gov/noaa-scales-explanation.

References

Banks, P. M. (1979). Joule heating in the high-latitude mesosphere. *Journal of Geophysical Research: Space Physics*, *84*(A11), 6709–6712. https://doi.org/10.1029/JA084iA11p06709

Burns, A. G., Killeen, T. L., Deng, W., Carignan, G. R., & Roble, R. G. (1995). Geomagnetic storm effects in the low- to middle-latitude upper thermosphere. *Journal of Geophysical Research: Space Physics*, *100*(A8), 14673–14691. https://doi.org/10.1029/94ja03232

Burns, A. G., Killeen, T. L., & Roble, R. G. (1992). Thermospheric heating away from the auroral oval during geomagnetic storms. *Canadian Journal of Physics*, *70*(7), 544–552. https://doi.org/10.1139/p92-089

Dawkins, E. C. M., Feofilov, A., Rezac, L., Kutepov, A. A., Janches, D., Höffner, J., et al. (2018). Validation of SABER v2.0 operational temperature data with ground-based lidars in the mesosphere-lower thermosphere region (75–105 km). *Journal of Geophysical Research: Atmospheres*, *123*(17), 9916–9934. https://doi.org/10.1029/2018JD028742

Esplin, R., Mlynczak, M. G., Russell, J., & Gordley, L. (2023). Sounding of the atmosphere using broadband emission radiometry (SABER): Instrument and science measurement description. *Earth and Space Science*, *10*(9). https://doi.org/10.1029/2023EA002999

Gonzalez-Esparza, J. A., Sanchez-Garcia, E., Sergeeva, M., Corona-Romero, P., Gonzalez-Mendez, L. X., Valdes-Galicia, J. F., et al. (2024). The Mother's Day geomagnetic storm on 10 May 2024: Aurora observations and low latitude space weather effects in Mexico. *Space Weather*, *22*(11), 1–17. https://doi.org/10.1029/2024SW004111

Killeen, T. L. (1987). Energetics and dynamics of the Earth's thermosphere. *Reviews of Geophysics*, *25*(3), 433–454. https://doi.org/10.1029/RG025i003p00433

Landry, R. G., & Anderson, P. C. (2019). Empirical modeling of the equatorward boundary of auroral precipitation using DMSP and DE 2. *Journal of Geophysical Research: Space Physics*, *124*(3), 2072–2082. https://doi.org/10.1029/2018JA025451

Lazzús, J. A., & Salfate, I. (2024). Report on the effects of the May 2024 Mother's day geomagnetic storm observed from Chile. *Journal of Atmospheric and Solar-Terrestrial Physics*, *261*(May), 106304. https://doi.org/10.1016/j.jastp.2024.106304

Lei, J., Thayer, J. P., Lu, G., Burns, A. G., Wang, W., Sutton, E. K., & Emery, B. A. (2011). Rapid recovery of thermosphere density during the October 2003 geomagnetic storms. *Journal of Geophysical Research: Space Physics*, *116*(3), 1–10. https://doi.org/10.1029/2010JA016164

Li, J., Wang, W., Lu, J., Yuan, T., Yue, J., Liu, X., et al. (2018). On the responses of mesosphere and lower thermosphere temperatures to geomagnetic storms at low and middle latitudes. *Geophysical Research Letters*, *45*(19), 10128–10137. https://doi.org/10.1029/2018GL078968

Li, J., Wang, W., Lu, J., Yue, J., Burns, A. G., Yuan, T., et al. (2019). A modeling study of the responses of mesosphere and lower thermosphere winds to geomagnetic storms at middle latitudes. *Journal of Geophysical Research: Space Physics*, *124*(5), 3666–3680. https://doi.org/10.1029/2019JA026533

Li, J., Wei, G., Wang, W., Luo, Q., Lu, J., Tian, Y., et al. (2023). A modeling study on the responses of the mesosphere and lower thermosphere (MLT) temperature to the initial and main phases of geomagnetic storms at high latitudes. *Journal of Geophysical Research: Atmospheres*, *128*(10), 1–14. https://doi.org/10.1029/2022JD038348

Liu, H., & Lühr, H. (2005). Strong disturbance of the upper thermospheric density due to magnetic storms: CHAMP observations. *Journal of Geophysical Research: Space Physics*, *110*(A9), 1–9. https://doi.org/10.1029/2004JA010908

Liu, H.-L. (2016). Variability and predictability of the space environment as related to lower atmosphere forcing. *Space Weather*, *14*(9), 634–658. https://doi.org/10.1002/2016SW001450

Liu, X., Yue, J., Wang, W., Xu, J., Zhang, Y., Li, J., et al. (2018). Responses of lower thermospheric temperature to the 2013 St. Patrick's Day geomagnetic storm. *Geophysical Research Letters*, *45*(10), 4656–4664. https://doi.org/10.1029/2018GL078039

Liu, X., Yue, J., Xu, J., Garcia, R. R., Russell, J. M., Mlynczak, M., et al. (2017). Variations of global gravity waves derived from 14 years of SABER temperature observations. *Journal of Geophysical Research: Atmospheres*, *122*(12), 6231–6249. https://doi.org/10.1002/2017JD026604

Liu, X., Yue, J., Xu, J., Wang, L., Yuan, W., Russell, J. M., & Hervig, M. E. (2014). Gravity wave variations in the polar stratosphere and mesosphere from SOFIE/AIM temperature observations. *Journal of Geophysical Research: Atmospheres*, *119*(12), 7368–7381. https://doi.org/10.1002/2013JD021439

Lübken, F. J., Höffner, J., Viehl, T. P., Kaifler, B., & Morris, R. J. (2011). First measurements of thermal tides in the summer mesopause region at Antarctic latitudes. *Geophysical Research Letters*, *38*(24), 10–13. https://doi.org/10.1029/2011GL050045

Matzka, J., Stolle, C., Yamazaki, Y., Bronkalla, O., & Morschhauser, A. (2021). The geomagnetic Kp index and derived indices of geomagnetic activity. *Space Weather*, *19*, e2020SW002641. Retrieved from https://kp.gfz-potsdam.de/

Mlynczak, M. G., Daniels, T., Hunt, L. A., Yue, J., Marshall, B. T., Russell, J. M., et al. (2020). Radiometric stability of the SABER instrument. *Earth and Space Science*, *7*(2), 1–8. https://doi.org/10.1029/2019EA001011

Mlynczak, M. G., Hunt, L. A., Garcia, R. R., Harvey, V. L., Marshall, B. T., Yue, J., et al. (2022). Cooling and contraction of the mesosphere and lower thermosphere from 2002 to 2021. *Journal of Geophysical Research: Atmospheres*, *127*(22), 1–17. https://doi.org/10.1029/2022JD036767

Mlynczak, M. G., Hunt, L. A., Nowak, N., Marshall, B. T., & Mertens, C. J. (2024). Global thermospheric infrared response to the Mother's Day weekend extreme storm of 2024. *Geophysical Research Letters*, *51*(15). https://doi.org/10.1029/2024GL110701

Mlynczak, M. G., Knipp, D. J., Hunt, L. A., Gaebler, J., Matsuo, T., Kilcommons, L. M., & Young, C. L. (2018). Space-based sentinels for measurement of infrared cooling in the thermosphere for space weather nowcasting and forecasting. *Space Weather*, *16*(4), 363–375. https://doi.org/10.1002/2017SW001757

Mlynczak, M. G., Marshall, B. T., Garcia, R. R., Hunt, L., Yue, J., Harvey, V. L., et al. (2023). Algorithm stability and the long-term geospace data record from TIMED/SABER. *Geophysical Research Letters*, *50*(5), 1–7. Retrieved from https://spdf.gsfc.nasa.gov/pub/data/timed/saber/

Mukhtarov, P., Pancheva, D., & Andonov, B. (2009). Global structure and seasonal and interannual variability of the migrating diurnal tide seen in the SABER/TIMED temperatures between 20 and 120 km. *Journal of Geophysical Research: Space Physics*, *114*(2), 1–17. https://doi.org/10.1029/2008JA013759

Pancheva, D., Singer, W., & Mukhtarov, P. (2007). Regional response of the mesosphere-lower thermosphere dynamics over Scandinavia to solar proton events and geomagnetic storms in late October 2003. *Journal of Atmospheric and Solar-Terrestrial Physics*, *69*(9), 1075–1094. https://doi.org/10.1016/j.jastp.2007.04.005

Pulkkinen, A., Lindahl, S., Viljanen, A., & Pirjola, R. (2005). Geomagnetic storm of 29-31 October 2003: Geomagnetically induced currents and their relation to problems in the Swedish high-voltage power transmission system. *Space Weather*, *3*(8). https://doi.org/10.1029/2004SW000123

Rees, M. H., Emery, B. A., Roble, R. G., & Stamnes, K. (1983). Neutral and ion gas heating by auroral electron precipitation. *Journal of Geophysical Research*, *88*(A8), 6289–6300. https://doi.org/10.1029/JA088iA08p06289

Remsberg, E. E., Marshall, B. T., Garcia-Comas, M., Krueger, D., Lingenfelser, G. S., Martin-Torres, J., et al. (2008). Assessment of the quality of the version 1.07 temperature-versus-pressure profiles of the middle atmosphere from TIMED/SABER. *Journal of Geophysical Research*, *113*(17), 1–27. https://doi.org/10.1029/2008JD010013

Richmond, A. D. (1979). Thermospheric heating in a magnetic storm: Dynamic transport of energy from high to low latitudes. *Journal of Geophysical Research: Space Physics*, *84*(A9), 5259–5266. https://doi.org/10.1029/JA084iA09p05259

Roble, R. G., Emery, B. A., Killeen, T. L., Reid, G. C., Solomon, S., Garcia, R. R., et al. (1987). Joule heating in the mesosphere and thermosphere during the July 13, 1982, solar proton event. *Journal of Geophysical Research: Space Physics*, *92*(A6), 6083–6090. https://doi.org/10.1029/ja092ia06p06083

Russell, J. M., III, Mlynczak, M. G., Gordley, L. L., Tansock, J. J., Jr., & Esplin, R. W. (1999). Overview of the SABER experiment and preliminary calibration results. In A. M. Larar (Ed.), *Optical spectroscopic techniques and instrumentation for atmospheric and space research III* (Vol. 3756, pp. 277–288). https://doi.org/10.1117/12.366382

Saroso, S., Iyemori, T., & Sugiura, M. (1993). Universal time variations in the ap and Dst Indices and their possible cause. *Journal of Geomagnetism and Geoelectricity*, *45*(7), 563–572. Retrieved from https://wdc.kugi.kyoto-u.ac.jp/

Shepherd, S. G. (2014). Altitude-adjusted corrected geomagnetic coordinates: Definition and functional approximations. *Journal of Geophysical Research: Space Physics*, *119*(9), 7501–7521. https://doi.org/10.1002/2014JA020264

Sun, M., Lu, J., Li, J., Tang, F., Wei, G., Li, Z., et al. (2024). Responses of mesosphere temperature to the geomagnetic storms on 8 and 15 September 2003. *Journal of Geophysical Research: Space Physics*, *129*(5), 1–12. https://doi.org/10.1029/2023JA032366

Tyssøy, H. N., Stadsnes, J., Sørbø, M., Mertens, C. J., & Evans, D. S. (2010). Changes in upper mesospheric and lower thermospheric temperatures caused by energetic particle precipitation. *Journal of Geophysical Research: Space Physics*, *115*(10), 1–11. https://doi.org/10.1029/2010JA015427

von Savigny, C., Sinnhuber, M., Bovensmann, H., Burrows, J. P., Kallenrode, M. B., & Schwartz, M. (2007). On the disappearance of noctilucent clouds during the January 2005 solar proton events. *Geophysical Research Letters*, *34*(2), 0–3. https://doi.org/10.1029/2006GL028106

Wang, N., Yue, J., Wang, W., Qian, L., Jian, L., & Zhang, J. (2021). A comparison of the CIR- and CME-induced geomagnetic activity effects on mesosphere and lower thermospheric temperature. *Journal of Geophysical Research: Space Physics*, *126*(6), 1–15. https://doi.org/10.1029/2020JA029029

Wang, W., Burns, A. G., Wiltberger, M., Solomon, S. C., & Killeen, T. L. (2008). Altitude variations of the horizontal thermospheric winds during geomagnetic storms. *Journal of Geophysical Research: Space Physics*, *113*(2), 1–17. https://doi.org/10.1029/2007JA012374

Wang, W., Talaat, E. R., Burns, A. G., Emery, B., Hsieh, S. Y., Lei, J., & Xu, J. (2012). Thermosphere and ionosphere response to subauroral polarization streams (SAPS): Model simulations. *Journal of Geophysical Research: Space Physics*, *117*(7), 1–18. https://doi.org/10.1029/2012JA017656

Wei, G., Lu, J., Tang, F., Li, J., & Sun, M. (2024). The dawn−dusk asymmetry in mesosphere and lower thermosphere temperature disturbances during geomagnetic storms at high latitude. *Earth and Planetary Physics*, *8*(2), 356–367. https://doi.org/10.26464/epp2024016

Xu, J., Smith, A. K., Liu, H. L., Yuan, W., Wu, Q., Jiang, G., et al. (2009). Seasonal and quasi-biennial variations in the migrating diurnal tide observed by Thermosphere, Ionosphere, Mesosphere, Energetics and Dynamics (TIMED). *Journal of Geophysical Research: Atmospheres*, *114*(13), 1–16. https://doi.org/10.1029/2008jd011298

Xu, J., Smith, A. K., Liu, M., Liu, X., Gao, H., Jiang, G., & Yuan, W. (2014). Evidence for nonmigrating tides produced by the interaction between tides and stationary planetary waves in the stratosphere and lower mesosphere. *Journal of Geophysical Research: Atmospheres*, *119*(2), 471–489. https://doi.org/10.1002/2013JD020150

Xu, J., Smith, A. K., Wang, W., Jiang, G., Yuan, W., Gao, H., et al. (2013). An observational and theoretical study of the longitudinal variation in neutral temperature induced by aurora heating in the lower thermosphere. *Journal of Geophysical Research: Space Physics*, *118*(11), 7410–7425. https://doi.org/10.1002/2013JA019144

Yamazaki, Y., Stolle, C., Stephan, C., & Mlynczak, M. G. (2024). Lower thermospheric temperature response to geomagnetic activity at high latitudes. *Journal of Geophysical Research: Space Physics*, *129*(7). https://doi.org/10.1029/2024JA032639

Yuan, T., Schmidt, H., She, C. Y., Krueger, D. A., & Reising, S. (2008). Seasonal variations of semidiurnal tidal perturbations in mesopause region temperature and zonal and meridional winds above Fort Collins, Colorado (40.6°N, 105.1°W). *Journal of Geophysical Research*, *113*(20), 1–12. https://doi.org/10.1029/2007JD009687

Yuan, T., She, C. Y., Hagan, M. E., Williams, B. P., Li, T., Arnold, K., et al. (2006). Seasonal variation of diurnal perturbations in mesopause region temperature, zonal, and meridional winds above Fort Collins, Colorado (40.6°N, 105°W). *Journal of Geophysical Research*, *111*(6), 1–17. https://doi.org/10.1029/2004JD005486

Zesta, E., & Oliveira, D. M. (2019). Thermospheric heating and cooling times during geomagnetic storms, including extreme events. *Geophysical Research Letters*, *46*(22), 12739–12746. https://doi.org/10.1029/2019GL085120

Zhang, X., Forbes, J. M., Hagan, M. E., Russell, J. M., Palo, S. E., Mertens, C. J., & Mlynczak, M. G. (2006). Monthly tidal temperatures 20-120 km from TIMED/SABER. *Journal of Geophysical Research: Space Physics*, *111*(10), 1–20. https://doi.org/10.1029/2005JA011504